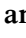**JFM** PAPERS

The role of vortex stretching in drag reduction of polymer-laden turbulent flow

Wouter J.T. Bos[1] , **Xuan Shao**[2,3] , **Tong Wu**[4] **and Le Fang**[2,3]

[1]CNRS, École Centrale de Lyon, INSA Lyon, LMFA, Université Claude Bernard Lyon 1, UMR5509, Écully 69134, France

[2]Laboratory of Complex Systems, Ecole Centrale de Pékin, Beihang University, Beijing 100191, PR China

[3]Research Institute of Aero-Engine, Beihang University, Beijing 100191, PR China

[4]Theoretical Physics I, University of Bayreuth, Universitätsstr. 30, Bayreuth 95447, Germany

Corresponding authors: Wouter J.T. Bos; Email: wouter.bos@ec-lyon.fr; Le Fang, le.fang@buaa.edu.cn

An addition of polymers can significantly reduce drag in wall-bounded turbulent flows, such as pipes or channels. This phenomenon is accompanied by a noticeable modification of the mean-velocity profile. Starting from the premise that polymers reduce vortex stretching, we derive a theoretical prediction for the mean-velocity profile. After assessing this prediction by numerical experiments of turbulence with reduced vortex stretching, we show that the theory successfully describes experimental measurements of drag reduction in pipe flow.

Key words: drag reduction, polymers, turbulent flows

1. Introduction

Turbulence rapidly drains energy from a fluid flow. Therefore, in many applications – such as aviation, naval and road transport and industrial processes – a significant portion of supplied energy is lost to undesired and difficult-to-control turbulent motion. Minimising turbulent drag is thus a key strategy for improving energetic efficiency. A spectacular example of turbulent drag reduction is an effect first experimentally studied by B.A. Toms in the 1940s (Toms 1949, 1977). Adding a small amount of polymers to a turbulent pipe or channel flow can reduce the turbulent drag enormously, leading thereby to important savings of energy.

Despite the large number of investigations dedicated to the subject (see reviews of older contributions in Lumley 1973 and Virk 1975 and more recent work in Procaccia,

L'vov & Benzi 2008, White & Mungal 2008; Xi 2019 and Dubief, Terrapon & Hof 2023), the precise effect remains obscure. It is realised that the polymers interact with turbulent velocity fluctuations in a certain way, which allows us to reduce the overall energy dissipation and the momentum flux from the fluid towards the wall. Early efforts of De Gennes and Lumley pointed to possible mechanisms associated with the elastic properties of polymers (De Gennes 1986; Tabor & De Gennes 1986) or the modification of the effective viscosity (Lumley 1973), an idea further explored, for instance, in L'vov *et al.* (2004) and Ryskin (1987*b*). More recent studies have focused on spatio-temporal intermittency, or hibernating states associated with events of reduced drag reduction (Graham 2004; Xi & Graham 2012; Whalley *et al.* 2017). Despite significant progress, none of these theories is entirely satisfactory or predictive.

Even though the precise mechanism behind turbulent drag reduction by polymers is unknown, the continued research efforts during eight decades have yielded a wealth of insights. Indeed, several key features of dilute polymer-containing flows near boundaries are now well established, and here we highlight some of these features.

Polymer-laden flows are visco-elastic, which adds to the difficulty of normal, viscous flows. Due to their elastic nature, the polymers need an extensional flow to get stretched. If the typical time scale of the flow is too large, the polymers will relax to their equilibrium coiled state. The dimensionless number which compares the elastic time scale with the flow time scale is called the Weissenberg number Wi. At low Weissenberg numbers, polymers have minimal influence on the flow.

As Wi increases beyond the coil–stretch transition (De Gennes 1974; Watanabe & Gotoh 2010), the drag reduction becomes more significant, reaching, for large enough values of Wi, an upper limit associated with a flow configuration known as the maximum drag reduction (MDR) state (Virk, Mickley & Smith 1970; Virk 1975). Notably, there appears to be a functional relationship between Wi and the extent of drag reduction in parallel shear flows (Owolabi, Dennis & Poole 2017). For large values of the drag reduction, and up to the MDR state, the mean-velocity profile in the near-wall region transitions from the logarithmic profile – characteristic of turbulent flow in Newtonian fluids – to a steeper profile. Historically, this profile was approximated using an alternative logarithmic expression (Virk 1975). However, more precise measurements have shown that the profile deviates from a logarithmic form (White, Dubief & Klewicki 2012), exhibiting a convex shape in log–linear representation (Ptasinski *et al.* 2001; Owolabi *et al.* 2017).

In this study, we focus on the role of vortex-stretching reduction in drag reduction. The importance of vortex stretching has been mentioned in numerous studies over the years. As early as the works of Gadd (1968) and Landahl (1973), vortex-stretching suppression was identified as a significant factor. Subsequent studies (Sureshkumar, Beris & Handler 1997; Yarin 1997) expanded on this idea, while experiments demonstrated that material-line stretching was reduced in polymer-laden flows (Liberzon *et al.* 2005). Recent numerical simulations confirm that polymers attenuate vortex stretching (ur Rehman *et al.* 2022), and experiments have shown that this attenuation is central to the mechanism of polymer drag reduction (Warwaruk & Ghaemi 2024).

Polymers reduce vortex stretching due to two key effects. First, it has been shown that rod-like passive particles or fibres align with the vorticity vector in turbulent flow (Pumir & Wilkinson 2011; Ni, Ouellette & Voth 2014), and this is expected to hold true for polymers as well. Second, the presence of polymers significantly increases the extensional viscosity (Metzner & Metzner 1970; Hinch 1977; Lindner, Vermant & Bonn 2003). From these two observations – the alignment of polymers with vorticity and the increased extensional viscosity – it follows that polymers attenuate vortex stretching. This attenuation reduces

drag since vortex stretching is one specific part of the nonlinear term, responsible for generating drag (Li *et al.* 2019).

The idea that drag reduction is linked to increased extensional viscosity is not new. Most theoretical studies acknowledge that this increase is a principal effect of polymers on visco-elastic flow. In purely extensional flows, this increase can be interpreted as an effective viscosity enhancement (Ryskin 1987*a*). When flows are not purely extensional, modifying the effective viscosity inhomogeneously provides a coarse model for the influence of polymers in wall-bounded flow, albeit without accounting for the difference between extensional and shear stresses. This approach underpins Lumley's theory (Lumley 1973), which can be refined using local energy balances and dimensional arguments to estimate viscosity changes (L'vov *et al.* 2004; Procaccia *et al.* 2008). However, firstly, this does not explain observations in homogeneous shear flow (Robert *et al.* 2010; Benzi & Ching 2018) where the viscosity should be statistically homogeneous and, secondly, turbulence is far from purely extensional. Incorporating a separate treatment of the two different stresses into the Navier–Stokes equations remains challenging. Only recently has progress been made on this for the case of two-dimensional flows (Oliveira 2024; see also Poole 2023).

The role of elasticity in polymer-laden turbulence is still a debated subject. At moderate and high Reynolds numbers it is the fully stretched polymers which are responsible for the drag reduction (Serafini *et al.* 2022), thereby suggesting that elastic effects are not necessary to explain drag reduction beyond the coil–stretch transition. However, around the MDR state, in particular at low Reynolds numbers, elastic instabilities might play an important role in maintaining a marginally unstable turbulent state (Choueiri, Lopez & Hof 2018; Dubief *et al.* 2023). We will come back to this point in the conclusion section. For the moment, we will ignore the effects of elasticity and consider flows beyond the coil–stretch transition.

In the present investigation, we avoid the complexities associated with altering the system's viscosity or modifying the viscous stress tensor. Instead, we focus directly on the vortex-stretching mechanism at the level of the governing equations. This approach neither relies on purely phenomenological arguments nor involves detailed simulations of visco-elastic turbulence. The strength of our method is its ability to isolate a specific aspect of polymer–turbulence interaction for specific analysis. Such an approach necessarily omits certain features of the interaction (such as elastic instabilities (Samanta *et al.* 2013) and the effect of the weight distribution of the polymers (Brandfellner *et al.* 2024; Serafini *et al.* 2025), etc.), but it will prove valuable since it allows us to derive an analytical prediction of the inertial velocity profile. We will then compare this prediction with specifically designed numerical experiments, before comparing it with laboratory experiments of polymer-laden turbulent pipe flow.

2. A law of the wall for turbulence with tamed vortex stretching

2.1. *Derivation of the mean profile*

To model the influence of reduced vortex stretching, we write the evolution equation of the fluid vorticity in the form

$$\frac{\partial \boldsymbol{\omega}}{\partial t} + \boldsymbol{u} \cdot \nabla \boldsymbol{\omega} = (1-\lambda)\boldsymbol{\omega} \cdot \nabla \boldsymbol{u} - \lambda \nabla P_{\omega} + \nu \Delta \boldsymbol{\omega}, \qquad (2.1)$$

where the vorticity $\boldsymbol{\omega}$ is the curl of the velocity $\boldsymbol{u}$, ν the kinematic viscosity and P_{ω} a Lagrange multiplier, ensuring $\nabla \cdot \boldsymbol{\omega} = 0$ (Wu, David & Bos 2023) λ is here a control

parameter which we will discuss below. A first property of this equation is that the left-hand side, representing the advection of the vorticity, is not modified. Intuitively, this represents the fact that the advection of a small fluid volume should be largely independent (at leading order) of what molecular particles, particles or fibres, the fluid particle contains. We hypothesise that this is different for the vortex-stretching term, since it is the term responsible for enstrophy generation, an effect dominated by extensional motion aligned with the vorticity. Indeed, the extensional stress is dramatically influenced by the presence of polymers in the flow.

In the case $\lambda = 0$ we retrieve the classical Navier–Stokes vorticity equation. The system (2.1) for $\lambda = 1$ was introduced in Bos (2021) and Wu & Bos (2021) and studied in statistically homogeneous flow. In the present investigation we consider (2.1) in wall-bounded flow as the simplest model for polymer-laden turbulence; we suppress vortex stretching, partially or completely, by allowing values $0 \leqslant \lambda \leqslant 1$.

Before carrying out numerical experiments, we will first extend the classical arguments of Prandtl and von Kármán (von Kármán 1930) to our system, in order to anticipate how the near-wall scaling is modified by the attenuation of vortex stretching. For this, we follow the same reasoning as von Kármán in his 1930 paper, which introduced the logarithmic law of the wall (or log law).

We focus on fully developed channel flow, with x, y, z the streamwise, wall-normal and spanwise directions, respectively. All average quantities are stationary and homogeneous in the streamwise and spanwise directions. The mean-velocity and vorticity fields are

$$\langle \boldsymbol{u} \rangle = U(y)\boldsymbol{e}_x \qquad \langle \boldsymbol{\omega} \rangle = -\frac{\mathrm{d}U(y)}{\mathrm{d}y}\boldsymbol{e}_z, \qquad (2.2)$$

respectively. From (2.1) we derive the exact mean vorticity balance $\partial_t \langle \omega_z \rangle$

$$0 = \lambda \frac{\mathrm{d}\langle \omega_z' v' \rangle}{\mathrm{d}y} + (\lambda - 1)\frac{d^2 \langle u'v' \rangle}{\mathrm{d}y^2} + \nu \frac{d^3 U}{\mathrm{d}y^3}. \qquad (2.3)$$

Neglecting viscous effects as usual in the derivation of the log law, we proceed by modelling the turbulent fluxes of mean vorticity and momentum, $\langle \omega_z' v' \rangle$ and $\langle u'v' \rangle$, using a classical mixing-length model

$$\langle a'v' \rangle = \nu_T \frac{\partial \langle a \rangle}{\partial y}, \text{ with } \nu_T = (\kappa y)^2 \left| \frac{\partial U}{\partial y} \right|, \qquad (2.4)$$

where a can be either the velocity or vorticity. This corresponds to a mixing length $l = \kappa y$ proportional to the distance to the wall (von Kármán 1930). In principle, different values can be used for the constant in the mixing-length estimate for vorticity or velocity (Hinze 1975), but this will not qualitatively change the outcome of this analysis. We obtain, since $\mathrm{d}\langle \omega_z \rangle/\mathrm{d}y = -\mathrm{d}^2 U/\mathrm{d}y^2$,

$$0 = \kappa^2 \lambda y^2 \frac{\mathrm{d}^2 U}{\mathrm{d}y^2}\frac{\mathrm{d}U}{\mathrm{d}y} + (1 - \lambda)\kappa^2 \frac{\mathrm{d}}{\mathrm{d}y}\left(y^2 \frac{\mathrm{d}U}{\mathrm{d}y}\frac{\mathrm{d}U}{\mathrm{d}y} \right). \qquad (2.5)$$

Equation (2.5) can be solved, yielding the solution

$$U^+(y^+) = \frac{1}{\kappa}\frac{y^{+\Gamma} - 1}{\Gamma} + U_0^+, \qquad (2.6)$$

with

$$\Gamma = \lambda/(2 - \lambda), \qquad (2.7)$$

where quantities are expressed in wall units ($U^+ = U/u_\tau$, with $u_\tau = (\nabla \langle p \rangle h/\rho)^{1/2}$, $y^+ = y u_\tau/\nu$) with ρ the density. In the derivation, an integration constant is fixed,
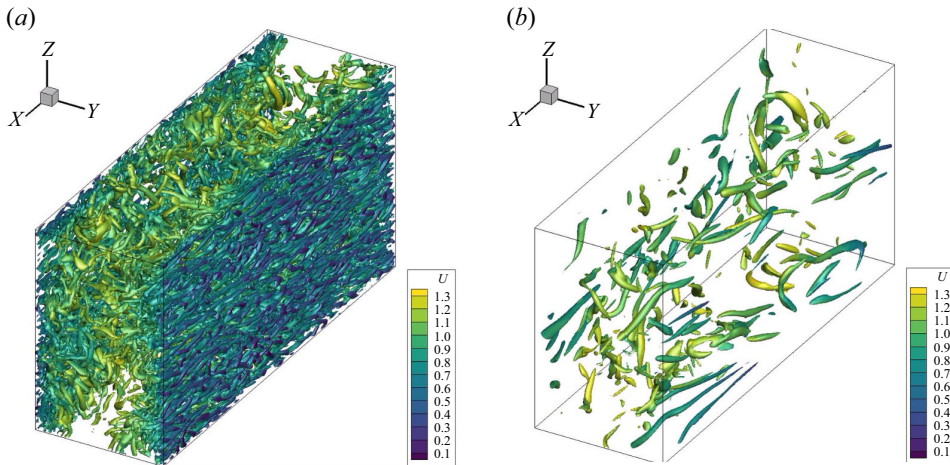
1019 A32-4

Figure 1. Plane-Poiseuille flow driven by an imposed pressure gradient in the x-direction. Vortical motion is amplified in three-dimensional turbulence by vortex stretching. The flow visualisations show iso-surfaces of the Q-criterion for $Q = 1$ (see main text), coloured by the local streamwise velocity. (*a*) Traditional channel flow. (*b*) Channel flow with reduced vortex stretching ($\lambda = 0.35$ in (2.1)).

as is customary, by the observation that, in the inertial layer of Newtonian channel flow turbulence, $|\langle u'v' \rangle| \approx u_\tau^2$ (Pope 2000).

According to this phenomenological analysis we thus find a power-law scaling with an exponent $\lambda/(2 - \lambda)$ for $0 < \lambda \leqslant 1$. For $\lambda = 0$ we find as a special case the logarithmic profile. Indeed, in the limit $\Gamma \downarrow 0$, we find that

$$\lim_{\Gamma \to 0} U^+(y^+) = \frac{1}{\kappa} \ln(y^+) + U_0^+. \tag{2.8}$$

The general λ-dependent mean-velocity profile (2.6) is the main analytical prediction which we will compare first with direct numerical simulations of (2.1) and subsequently with experimental results from literature on polymer turbulence.

2.2. *Numerical experiments of turbulence with reduced vortex stretching*

To assess our predictions, we carry out Direct Numerical Simulations (DNS) of (2.1) in plane channel flow. The walls are separated by a width $2h$, the width of the domain is πh and the length $2\pi h$. Boundary conditions are no slip at the wall and periodic in the stream-wise and spanwise directions. The code is based on a classical Fourier–Chebyshev formulation with a resolution of $N_x = 256$, $N_y = 192$, $N_z = 192$ grid points. Further details can be found in Appendix A. Computations are carried out for $R_\tau = 395$ at a constant mass-flow rate. Simulations are run until a statistically steady state is obtained for the Navier–Stokes case $\lambda = 0$, as measured by observing the wall shear stress. Starting from this steady state, λ is varied in the range $\lambda \in [0, 0.5]$ with steps of $\delta\lambda = 0.05$. For simulations with $\lambda \leqslant 0.35$ turbulent steady states are observed, while for $\lambda \geqslant 0.4$ the flows relaminarise.

In figure 1 we show flow visualisations using the Q-criterion (Hunt, Wray & Moin 1988) for $Q \equiv \Delta p/2 = 1$. Comparing the Navier–Stokes case (*a*) with the case $\lambda = 0.35$ (*b*), it is observed that, in the second case, the vortex intensity has reduced dramatically. Indeed, the vortex-stretching term is responsible for enstrophy production, and reducing it leads to the intuitive effect of less vortical activity.

In figure 2(*a*) we show mean-velocity profiles for the turbulent cases, determined by averaging during the statistically steady state. Also shown is our prediction, where $\kappa = 0.4$
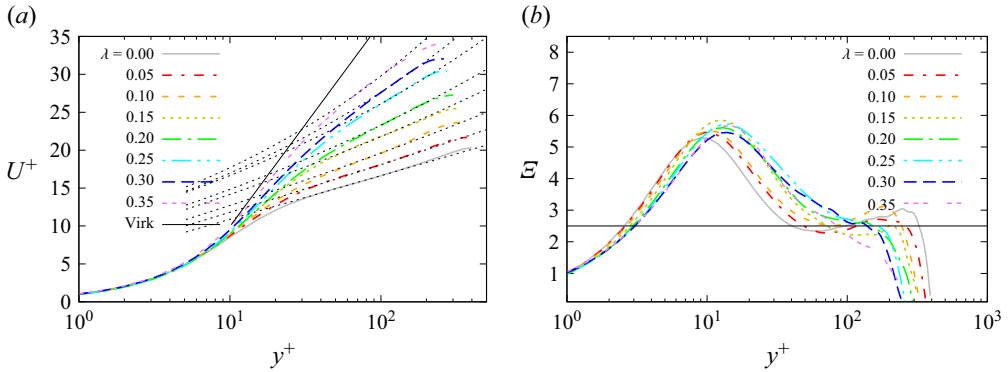
Figure 2. Comparison of analytical predictions with our DNS results. (*a*) Mean-velocity profiles in log–linear representation. The values of U_0^+ are for $\lambda \in [0, 0.35]$: 5.1; 5.9; 6.6; 7.8; 8.3; 9.8; 9.9; 10.3. (*b*) The generalised indicator function $\varXi = (y^+)^{1-\lambda/(2-\lambda)} dU^+(y^+)/dy^+$, (2.10) for the different velocity profiles in (*a*).

and the only adjustable parameter is the velocity offset $U_0^+(\lambda)$, which is fitted to obtain a best fit in the region where the generalised indicator function (see below) is in the vicinity of $1/\kappa$. Even though the Reynolds number is rather small, the predicted profiles describe the data well. The relation between the values $U_0^+(\lambda)$ and λ is approximately linear

$$U_0^+(\lambda) = U_0^+(0) + \lambda b_U, \tag{2.9}$$

with $U_0^+(0) = 5.2 \pm 0.2$ and $b_U = 15.8 \pm 1$.

In order to assess our predictions independently from the virtual origin $U_0(\lambda)$, we introduce a generalised indicator function

$$\varXi[U, y] = y^{1-\Gamma} \frac{dU(y)}{dy}, \tag{2.10}$$

where $\Gamma = \lambda/(2 - \lambda)$. For the value $\lambda = 0$ this simplifies to the commonly used indicator function to verify the existence of a logarithmic profile (e.g. White *et al.* 2012; Laadhari 2019). For $\lambda \neq 0$, this function should allow us to identify the power-law behaviour (2.6) by a plateau of value $1/\kappa$ independently of the adjustable parameters other than the value of λ, which is fixed for each simulation.

Even though the Reynolds number is too low to have a substantial inertial profile, figure 2(*b*) shows that all 7 simulations coincide near the value $1/\kappa \approx 2.5$ around $y^+ = 100$, supporting the idea that κ plays a central role, irrespective of the amount of vortex stretching that is suppressed in the governing equations.

3. Drag reduction and vortex stretching

3.1. *Similarities between the modified Navier–Stokes equations and visco-elastic turbulence*

The extended von Kármán phenomenology appears to capture the behaviour of (2.1), elucidating how reduced vortex stretching modifies the mean-velocity profile. The next question is: How relevant is (2.1) for modelling polymer turbulence?

Since (2.1) lacks derivation from a polymer stress constitutive relation (an important question for future research), its relevance must be inferred by comparing its properties with those of real flows. Before attempting such comparison, let us discuss certain similarities between polymer-laden turbulence and (2.1).
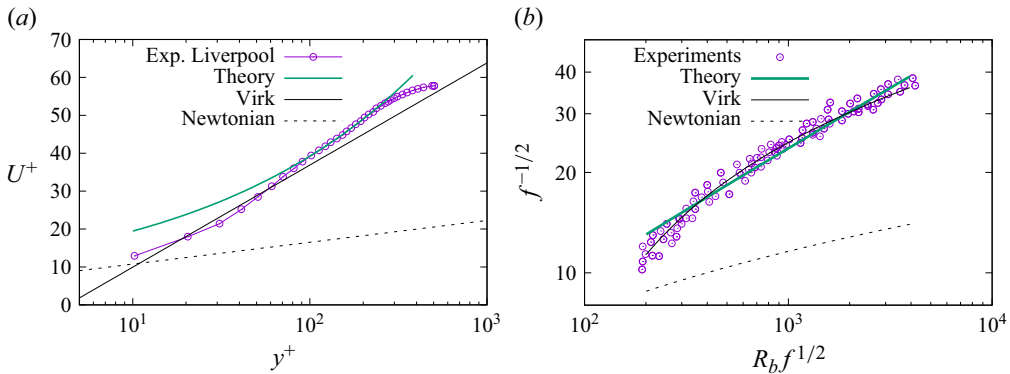
Figure 3. Comparison of analytical predictions with experimental results. (*a*) Mean-velocity profile in pipe flow at MDR (Owolabi *et al.* 2017) compared with our power-law estimate. (*b*) Fanning friction factor in Prandtl–von Karman coordinates. Experimental results from smooth pipe measurements at MDR (Virk *et al.* 1970).

First, the steepened velocity profile in our system qualitatively resembles profiles in polymer turbulence. Although our approach does not model the coil–stretch transition (De Gennes 1974), the continuous profile steepening aligns with high drag reduction regimes (Warholic, Massah & Hanratty 1999).

Second, our system stabilises at a marginally stable state for $\lambda \approx 0.35$, with relaminarisation at higher values. While polymer turbulence also reaches an asymptotic (MDR) state, the flow does not relaminarise at high Reynolds numbers. It is plausible that exceeding MDR suppresses vortex stretching to the point of relaminarisation, at which polymers relax to their coiled equilibrium state. This would cause the flow to revert to Newtonian-like properties, reintroducing instabilities and turbulence. Local spatio-temporal relaminarisation could correspond to hibernating turbulent states (Graham 2004; Xi & Graham 2012).

Third, drag reduction can occur for both elastic and rod-like polymers (Berman 1978; Paschkewitz *et al.* 2004; Japper-Jaafar, Escudier & Poole 2009), suggesting that polymer-induced drag reduction is not purely elastic in origin. Our approach, lacking relaxation time scales (inherent to elastic effects) is consistent with this observation.

Fourth, simulations of visco-elastic isotropic turbulence and turbulence without vortex stretching reveal shared features. Simulations employing the finite extensible nonlinear elastic model with Peterlin's approximation show that, at high Weissenberg numbers, the kinetic energy spectrum transitions from a $k^{-5/3}$ scaling to k^{-3}, with k the wavenumber (Valente *et al.* 2014, 2016), as also observed in channel flows (Mitishita, Elfring & Frigaard 2023). This k^{-3} scaling, linked to enstrophy conservation, is similarly observed in turbulence without vortex stretching (Wu & Bos 2022). Furthermore, advanced simulations (Watanabe & Gotoh 2013) demonstrate that polymers suppress enstrophy production, promoting a conservative enstrophy cascade at high Reynolds numbers.

These similarities motivate further scrutiny of the connection between polymer drag reduction and (2.1). We therefore compare its predictions with experimental results.

3.2. *Comparison with experiments of visco-elastic shear flow*

We compare our predictions with measures in pipe flow, which is, historically, the most investigated case. We first compare with the velocity profile in pipe flow at MDR measured experimentally at the University of Liverpool (Owolabi *et al.* 2017) in figure 3(*a*). Fitting

our prediction (2.6) in the range $100 \leqslant y^+ \leqslant 250$, we obtain $\Gamma \equiv \lambda/(2 - \lambda) = 0.349 \pm 0.001$ and $U_0^+ = 3.5 \pm 0.13$. Agreement at these scales is convincing and clearly superior to Virk's approximation.

A larger amount of data are available on the friction factor, which is more easily measured in experiments. We will here compare with the pioneering compilation of results by Virk *et al.* (1970). The friction factor is determined by measuring the pressure drop δp over a pipe of length L. Introducing the bulk velocity U_b (velocity averaged over the pipe cross-section of radius R) the friction factor is

$$f = 2 \left(\frac{u_\tau}{U_b} \right)^2 , \tag{3.1}$$

where $u_\tau = \sqrt{R \delta p / (2 \rho L)}$. Experiments are then performed to measure the value of f as a function of the bulk Reynolds number, $R_b = 2 R U_b / \nu$. Results are traditionally plotted, in Prandtl–von Kármán representation, $f^{-1/2}$ as a function of $R_b f^{1/2} (= 2\sqrt{2} R_\tau)$.

We determine the bulk velocity by integrating the velocity profile over the pipe cross-section, yielding, after a change of variables $r = R - y$ and $y^+ = ((R - r)/R) R_\tau$, the relation

$$f^{-1/2} = \frac{\sqrt{2}}{R_\tau} \int_0^{R_\tau} \left(1 - \frac{y^+}{R_\tau} \right) U^+(y^+) \mathrm{d}y^+ . \tag{3.2}$$

We now use expression (2.6) for $\lambda \neq 0$, to obtain

$$f^{-1/2} = \frac{2 \left(\left[R_b f^{1/2} / \sqrt{8} \right]^\Gamma - 1 \right) / \Gamma - (\Gamma + 3)}{\sqrt{2} \kappa (\Gamma + 1)(\Gamma + 2)} + \frac{U_0^+}{\sqrt{2}} . \tag{3.3}$$

We show this expression in figure 3(*b*). Fitting the data we find $\Gamma = 0.348 \pm 0.003$ and $U_0^+ = 5.6 \pm 0.4$. Also shown are the Newtonian expression $f^{-1/2}(x) = 4 \log(x) - 0.4$ and Virk's relation $f^{-1/2}(x) = 19 \log(x) - 32.4$.

What we can say is that, for large values of the Reynolds number, the agreement between experiments of the friction factor and our theory is at least as good as using Virk's log law, with the difference that our fit is based on a theoretical expression for the velocity profile (2.6), valid for both Newtonian and visco-elastic flow, whereas Virk's expression is an empirical fit to the MDR data. For the velocity profile for the scales $100 < y^+ < 250$ the agreement with our theory is clearly superior (figure 3*a*).

It is remarkable that we obtain, within error bars, exactly the same value for Γ in figures 3(*a*) and 3(*b*). This supports the validity of (2.6) to describe the mean profile at MDR. The slightly different value of U_0 is not surprising since we obtain the estimate for U_b by integrating over the full pipe cross-section, although the power law does not hold for y^+ near the wall and the centre. Another nice feature is that (3.3) holds also for the Newtonian case, when the value $\Gamma = 0$ is used.

A question we have not addressed is the link between the Weissenberg number and the vortex-stretching parameter λ. At present, we have no direct physical relation between λ and Wi derived from a visco-elastic constitutive relation. In order to obtain a tentative link, we compare the results of our system with the compilation of Owolabi *et al.* (2017), who showed that the amount of drag reduction in different pipes and channels could be linked by a close-to-universal relation to Wi. The drag reduction, for a fixed mass-flow
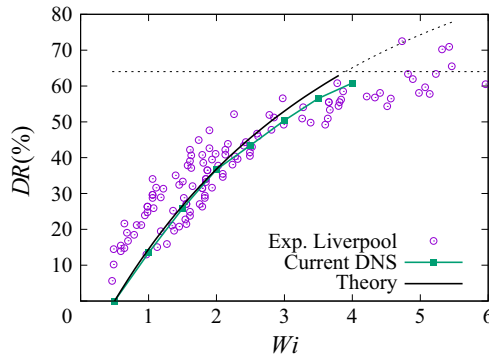
Figure 4. Drag reduction as a function of the Weissenberg number. Comparison of experimental results of Owolabi *et al.* (2017) with our analytical predictions and numerical results for DNS with reduced vortex stretching. For the comparison we use a linear relation, $Wi - Wi_c = 10\lambda$ between the reduction of vortex stretching λ and Wi. The horizontal dashed line represents the MDR value ($DR = 64\%$) corresponding to the fit to the experimental results in Owolabi *et al.* (2017).

rate, is defined as

$$DR = \left(1 - \left(\frac{u_\tau}{u_\tau^{(0)}}\right)^2\right), \tag{3.4}$$

where $u_\tau^{(0)}$ is the friction velocity for the reference case. In figure 4 we show the experimental data points for the interval $0 < Wi < 6$. We compare with the results of our DNS for different values of λ. To attempt a comparison and in the absence of a physical model, we try to compare the data using the linear relation

$$Wi - Wi_c = a\lambda, \tag{3.5}$$

which is the simplest possible non-trivial relation, taking into account that the suppression of vortex stretching should increase with the Weissenberg number, at least for values between the coil–stretch transition (at the critical Weissenberg number Wi_c) and MDR. We use the value $Wi_c = 0.5$ and the value $a = 10$, which seem to give a good qualitative agreement.

To compare with the theory, we integrate the mean-velocity profile (2.6) over half of the channel to get an estimate of the bulk velocity

$$\begin{aligned} U_b &= \frac{u_\tau}{h} \int_0^h U(y)\mathrm{d}y \\ &= \frac{u_\tau}{\kappa(\Gamma + 1)} \left[\frac{\left(\frac{hu_\tau}{\nu}\right)^\Gamma - 1}{\Gamma} - 1\right] + u_\tau U_0(\lambda), \end{aligned} \tag{3.6}$$

yielding an implicit equation for u_τ for fixed U_b, which can be numerically solved, using (2.9). The resulting values of u_τ are used to compute the drag reduction, shown in figure 4. The tendency is the same as the DNS and the experiments. Quantitative disagreement with the DNS can be attributed to the assumption of using (2.6) over the complete channel, ignoring deviations near the wall and centre of the domain. Using this relation between λ and Wi, we find that the value $\Gamma = 0.349$ we obtained in figure 3 corresponds to $Wi_{MDR} \approx 5.6$, which is not inconsistent with the results in Owolabi *et al.* (2017).

4. Conclusion and future issues

The complexity of polymer-laden turbulence is rooted in the multi-scale interaction of turbulence with polymer molecules (Koide & Goto 2024) combined with the presence of walls, introducing both scale and position dependences. While advanced numerical experiments now provide access to detailed flow quantities in realistic geometries (Serafini *et al.* 2022), progress in understanding requires drastic simplifications of the flow physics to isolate specific features – an approach we have adopted.

Introducing the new system of governing equations (2.1) for the investigation of drag reduction by polymers opens several avenues for exploration. A first and important one is the assessment of the assumption that strong extensional viscosity primarily acts to damp the term $\boldsymbol{\omega} \cdot \nabla \boldsymbol{u}$ in the vorticity dynamics. Such an assessment could start from the framework introduced in Oliveira (2024). Further comparisons should investigate the implications of (2.1) for the detailed inhomogeneous and anisotropic turbulence statistics (Escudier, Nickson & Poole 2009).

Perhaps even more intriguingly, investigating the self-sustaining mechanism of wall turbulence (De Angelis *et al.* 2002; Waleffe 1997) and the linear and nonlinear instability properties of shear flows with reduced vortex stretching, could provide theoretical insights into the nature of the MDR state. While at low Reynolds numbers certain results indicate that elastic instabilities might determine the precise asymptotic value of MDR (Dubief *et al.* (2023) and references therein), this question is not settled at high Reynolds numbers. The MDR asymptote at higher Reynolds numbers might be determined by a subcritical transition (Morozov & van Saarloos 2005, 2007), and as such, its precise value is certainly not easy or impossible to determine by simple analytical reasoning.

In this context, an interesting observation in our study is that we observe laminarisation at relatively large values of the Reynolds number for sufficiently high values of λ, in the absence of elastic effects. Let us imagine what elastic effects would add in such a relaminarised state in an actual visco-elastic fluid. There, polymers would relax back to their equilibrium state, which would have two direct influences: first, the relaxation could reintroduce kinetic energy into the flow when the polymer stress changes sign, as observed in isotropic visco-elastic turbulence (Nguyen *et al.* 2016; Valente, Da Silva & Pinho 2014) at small scales and high Weissenberg number, or in low Reynolds number shear flows due to elastic instabilities Choueiri *et al.* (2018). This energy flux could possibly perturb the relaminarised state. Second, after relaxation, the extensional viscosity would recover its Newtonian value and the flow would become unstable again. Both effects would contribute to sustaining a marginally unstable state, which would act as a visco-elastic fluid at the MDR asymptote.

These arguments support the ideas that, firstly, (extensionally) viscous effects are the main actor in reaching the MDR state. Secondly, that elastic effects are essential to maintain a turbulent state once the MDR asymptote is reached. A more sophisticated model than (2.1) is needed to assess this reasoning and the development of such a model is left for further research.

Declaration of interests. The authors report no conflict of interest.

Appendix A. Numerical method

We carry out simulations of plane-Poiseuille flow. The half-width of the channel is denoted h, the computational domain has dimensions of $L_x \times L_y \times L_z = 2\pi h \times 2h \times \pi h$ and employs $N_x \times N_y \times N_z = 256 \times 192 \times 192$ grid points. Uniform grids are applied in the streamwise and spanwise directions, while a non-uniform grid is used in the wall-normal (y) direction, defined by $y_j = \cos(\pi j/N_y)$ for $j = 0, 1, \ldots, N_y$. Note that in the numerical method $y = 0$ is the centreline of the channel. The initial mean-velocity profile is set as $U(y) = (3F/4)(1 - y^2)$. By maintaining a constant mass-flow rate $F = 2$, the flow achieves a Reynolds number of $R_\tau = h u_\tau/\nu = 395$, with ν the kinematic viscosity and $u_\tau = \sqrt{\tau_w/\rho}$ the friction velocity. Here, τ_w represents wall shear stress and ρ denotes density.

We conduct simulations with different values of λ, starting from a fully developed flow of conventional Navier–Stokes turbulence ($\lambda = 0$). The numerical method for conventional turbulence has been validated in previous studies (Xu, Zhang & Nieuwstadt 1996; Fang *et al.* 2011; Chen & Fang 2024). Spatial discretisation is conducted using the Fourier–Galerkin and Chebyshev–Gauss–Lobatto collocation methods: streamwise and spanwise directions are expanded using Fourier series, while the wall-normal direction utilises Lagrange interpolation polynomials at Chebyshev–Gauss–Lobatto collocation points.

Before explaining the time advancement, let us start by formulating the evolution equation for the velocity. Equation (A1) of the manuscript is formulated for the evolution of the vorticity, whereas the numerical method we use is based on the time advancement of the velocity. We therefore use the Biot–Savart operator to write

$$\frac{\partial \boldsymbol{u}}{\partial t} = \Delta^{-1} \boldsymbol{\nabla} \times \left(\frac{\partial \boldsymbol{\omega}}{\partial t} \right). \tag{A1}$$

We now write two evolution equations. The first equation corresponds to Navier–Stokes turbulence

$$\begin{cases} \dfrac{\partial \boldsymbol{u}}{\partial t} = \boldsymbol{u} \times \boldsymbol{\omega} - \boldsymbol{\nabla} \Pi + \nu \nabla^2 \boldsymbol{u}, \\ \Pi = \dfrac{\boldsymbol{u} \cdot \boldsymbol{u}}{2} + \dfrac{p}{\rho}. \end{cases} \tag{A2}$$

The second one corresponds to turbulence without vortex stretching

$$\begin{cases} \dfrac{\partial \boldsymbol{u}}{\partial t} = \Delta^{-1} \boldsymbol{\nabla} \times ((\boldsymbol{u} \cdot \boldsymbol{\nabla})\boldsymbol{\omega}) - \boldsymbol{\nabla} \Pi + \nu \nabla^2 \boldsymbol{u}, \\ \Pi = \dfrac{\boldsymbol{u} \cdot \boldsymbol{u}}{2} + \dfrac{p}{\rho}, \end{cases} \tag{A3}$$

where we used (A1). Adding now the first and the second equation in proportions λ and $1 - \lambda$, we obtain the evolution of the velocity with partially removed vortex stretching

$$\begin{cases} \dfrac{\partial \boldsymbol{u}}{\partial t} = \lambda \left(\Delta^{-1} \boldsymbol{\nabla} \times ((\boldsymbol{u} \cdot \boldsymbol{\nabla})\boldsymbol{\omega}) \right) + (1 - \lambda)(\boldsymbol{u} \times \boldsymbol{\omega}) \\ \qquad\qquad - \boldsymbol{\nabla} \Pi + \nu \nabla^2 \boldsymbol{u}, \\ \Pi = \dfrac{\boldsymbol{u} \cdot \boldsymbol{u}}{2} + \dfrac{p}{\rho}. \end{cases} \tag{A4}$$

Now that we have a velocity-evolution equation we will describe the time advancement in detail.

The time-advancement scheme is based on a semi-implicit, three-step backward differentiation formula (that is, $J_e = 3$) (Moin, Reynolds & Ferziger 1978; Fan & Dong 2022). During each time step, a third-order time-splitting method is employed, including three substeps that sequentially process the convective, pressure and diffusion terms, respectively. In the following parts, superscripts s, $s + (1/3)$, $s + (2/3)$ and $s + 1$ will be used to denote the advancement from time step s to $s + 1$, corresponding to the substeps, respectively.

In the present work without vortex stretching, the convective term in (A4) is advanced from s to $s + (1/3)$ using two microsteps, by further introducing an instant $s + (1/6)$. The first microstep indicates the influence of the term $\lambda(\Delta^{-1}\nabla \times ((\boldsymbol{u} \cdot \nabla)\boldsymbol{\omega}))$, written as

$$\frac{\Delta \boldsymbol{u}^{s+\frac{1}{6}} - \sum_{q=0}^{J_e-1} \alpha_q \Delta \boldsymbol{u}^{s-q}}{\mathrm{d}t} = \sum_{q=0}^{J_e-1} \gamma_q \left[\lambda(\nabla \times (\boldsymbol{u} \cdot \nabla)\boldsymbol{\omega})\right]^{s-q}, \tag{A5}$$

with no-slip boundary conditions

$$\left\{ u_{y=\pm1} = v_{y=\pm1} = w_{y=\pm1} = 0 \right. . \tag{A6}$$

The second microstep indicates the influence of the term $(1 - \lambda)(\boldsymbol{u} \times \boldsymbol{\omega})$

$$\frac{\boldsymbol{u}^{s+\frac{1}{3}} - \boldsymbol{u}^{s+\frac{1}{6}}}{\mathrm{d}t} = \sum_{q=0}^{J_e-1} \gamma_q \left[(1 - \lambda)(\boldsymbol{u} \times \boldsymbol{\omega})\right]^{s-q}, \tag{A7}$$

with additional boundary conditions

$$\frac{\boldsymbol{u}^{s+\frac{1}{3}} - \sum_{q=0}^{J_e-1} \alpha_q \boldsymbol{u}^{s-q}}{\mathrm{d}t} = \sum_{q=0}^{J_e-1} \gamma_q \left[(1 - \lambda)(\boldsymbol{u} \times \boldsymbol{\omega})\right]^{s-q}. \tag{A8}$$

The calculation of the pressure term in (A4) (from $s + (1/3)$ to $s + (2/3)$) advances as

$$\left\{ \begin{array}{l} \dfrac{\boldsymbol{u}^{s+\frac{2}{3}} - \boldsymbol{u}^{s+\frac{1}{3}}}{\mathrm{d}t} = -\nabla \Pi^{s+\frac{2}{3}}, \\ \qquad \nabla \cdot \boldsymbol{u}^{s+\frac{2}{3}} = 0, \end{array} \right. \tag{A9}$$

for the internal field, with the wall boundary condition for the pressure step modified as

$$\left(\nabla \Pi^{s+\frac{2}{3}}\right) \cdot \boldsymbol{e_y} = \left(\sum_{q=0}^{J_e-1} \gamma_q \left[(1 - \lambda)(\boldsymbol{u} \times \boldsymbol{\omega})\right]^{s-q} + \nu \sum_{q=0}^{J_e-1} \gamma_q \left(-\nabla \times \left(\nabla \times \boldsymbol{u}^{s-q}\right)\right) \right) \cdot \boldsymbol{e_y}, \tag{A10}$$

where (A10) involves the unit normal vector $\boldsymbol{e_y}$. The coefficients in (A5), (A7), (A6), (A8) and (A10) remain consistent with conventional Navier–Stokes turbulence in the case $\lambda = 0$.

The viscous term, advancing from time step $s + (2/3)$ to $s + 1$, is

$$\frac{\gamma_3 \boldsymbol{u}^{s+1} - \boldsymbol{u}^{s+\frac{2}{3}}}{\mathrm{d}t} = \nu \nabla^2 \boldsymbol{u}^{s+1}. \tag{A11}$$

The coefficients in the semi-implicit scheme α_0, α_1, α_2, γ_0, γ_1, γ_2 and γ_3 are reported in Karniadakis, Israeli & Orszag (1991).

REFERENCES

BENZI, R. & CHING, E.S.C. 2018 Polymers in fluid flows. *Annu. Rev. Condens. Matter Phys.* **9** (1), 163–181.

BERMAN, N.S. 1978 Drag reduction by polymers. *Annu. Rev. Fluid Mech.* **10** (1), 47–64.

BOS, W.J.T. 2021 Three-dimensional turbulence without vortex stretching. *J. Fluid Mech.* **915**, A121.

BRANDFELLNER, L., MURATSPAHIĆ, E., BISMARCK, A. & MÜLLER, H.W. 2024 Quantitative description of polymer drag reduction: effect of polyacrylamide molecular weight distributions. *J. Non-Newtonian Fluid Mech.* **325**, 105185.

CHEN, Z.H. & FANG, L. 2024 Eliminating the residual velocity divergence of spectral methods in channel turbulence. *Prog. Comput. Fluid Dyn.* **24** (3), 127.

CHOUEIRI, G.H., LOPEZ, J.M. & HOF, B. 2018 Exceeding the asymptotic limit of polymer drag reduction. *Phys. Rev. Lett.* **120** (12), 124501.

DE ANGELIS, E., CASCIOLA, C.M. & PIVA, R. 2002 Dns of wall turbulence: dilute polymers and self-sustaining mechanisms. *Comput. Fluids* **31** (4–7), 495–507.

DE GENNES, P.G. 1974 Coil-stretch transition of dilute flexible polymers under ultrahigh velocity gradients. *J. Chem. Phys.* **60** (12), 5030–5042.

DE GENNES, P.G. 1986 Towards a scaling theory of drag reduction. *Physica A: Stat. Mech. Applics.* **140** (1–2), 9–25.

DUBIEF, Y., TERRAPON, V.E. & HOF, B. 2023 Elasto-inertial turbulence. *Annu. Rev. Fluid Mech.* **55** (1), 675–705.

ESCUDIER, M.P., NICKSON, A.K. & POOLE, R.J. 2009 Turbulent flow of viscoelastic shear-thinning liquids through a rectangular duct: quantification of turbulence anisotropy. *J. Non-Newtonian Fluid Mech.* **160** (1), 2–10.

FAN, B. & DONG, G. 2022 *Principles of Turbulence Control*. John Wiley & Sons.

FANG, L., SHAO, L., BERTOGLIO, J.P., LU, L.P. & ZHANG, Z.S. 2011 The rapid-slow decomposition of the subgrid flux in inhomogeneous scalar turbulence. *J. Turbul.* **12**, N8.

GADD, G.E. 1968 Effects of drag-reducing additives on vortex stretching. *Nature* **217** (5133), 1040–1042.

GRAHAM, M.D. 2004 Drag reduction in turbulent flow of polymer solutions. *Rheol. Rev.* **2** (2), 143–170.

HINCH, E.J. 1977 Mechanical models of dilute polymer solutions in strong flows. *Phys. Fluids* **20** (10), S22–S30.

HINZE, J.O. 1975 *Turbulence*. McGraw-Hill.

HUNT, J.C.R., WRAY, A.A. & MOIN, P. 1988 Eddies, streams, and convergence zones in turbulent flows. In *Studying Turbulence using Numerical Simulation Databases, 2. Proceedings of the 1988 Summer Program*. Stanford University.

JAPPER-JAAFAR, A., ESCUDIER, M.P. & POOLE, R.J. 2009 Turbulent pipe flow of a drag-reducing rigid 'rod-like' polymer solution. *J. Non-Newtonian Fluid Mech.* **161** (1–3), 86–93.

VON KÁRMÁN, T. 1930 Mechanische änlichkeit und turbulenz. *Nachr. Ges. Wiss. Göttingen Mathematisch-Physikalische Klasse* **1930**, 58–76.

KARNIADAKIS, G.E., ISRAELI, M. & ORSZAG, S.A. 1991 High-order splitting methods for the incompressible Navier–Stokes equations. *J. Comput. Phys.* **97** (2), 414–443.

KOIDE, Y. & GOTO, S. 2024 Polymer stretching and alignment under the hierarchy of coherent vortices in turbulence. *Phys. Rev. Fluids* **9** (12), 123303.

LAADHARI, F. 2019 Refinement of the logarithmic law of the wall. *Phys. Rev. Fluids* **4** (5), 054605.

LANDAHL, M.T. 1973 Drag reduction by polymer addition. In *Theoretical and Applied Mechanics: Proceedings of the 13th International Congress of Theoretical and Applied Mechanics, Moskow University, August 21–16, 1972*, pp. 177–199. Springer.

LI, W., FAN, Y., MODESTI, D. & CHENG, C. 2019 Decomposition of the mean skin-friction drag in compressible turbulent channel flows. *J. Fluid Mech.* **875**, 101–123.

LIBERZON, A., GUALA, M., LÜTHI, B., KINZELBACH, W. & TSINOBER, A. 2005 Turbulence in dilute polymer solutions. *Phys. Fluids* **17** (3), 031707.

LINDNER, A., VERMANT, J. & BONN, D. 2003 How to obtain the elongational viscosity of dilute polymer solutions? *Physica A: Stat. Mech. Applics.* **319**, 125–133.

LUMLEY, J.L. 1973 Drag reduction in turbulent flow by polymer additives. *J. Polym. Sci.: Macromol. Rev.* **7** (1), 263–290.

L'VOV, V.S., POMYALOV, A., PROCACCIA, I. & TIBERKEVICH, V. 2004 Drag reduction by polymers in wall bounded turbulence. *Phys. Rev. Lett.* **92** (24), 244503.

METZNER, A.B. & METZNER, A.P. 1970 Stress levels in rapid extensional flows of polymeric fluids. *Rheol. Acta* **9**, 174–181.

MITISHITA, R.S., ELFRING, G.J. & FRIGAARD, I.A. 2023 Statistics and spectral analysis of turbulent duct flows with flexible and rigid polymer solutions. *J. Non-Newtonian Fluid Mech.* **311**, 104952.

MOIN, P., REYNOLDS, W.C. & FERZIGER, J.H. 1978 Large eddy simulation of incompressible turbulent channel flow. *Tech. Rep*. No. NASA-CR-152190. Stanford University.

MOROZOV, A.N. & VAN SAARLOOS, W. 2005 Subcritical finite-amplitude solutions for plane Couette flow of viscoelastic fluids. *Phys. Rev. Lett.* **95** (2), 024501.

MOROZOV, A.N. & VAN SAARLOOS, W. 2007 An introductory essay on subcritical instabilities and the transition to turbulence in visco-elastic parallel shear flows. *Phys. Rep.* **447** (3–6), 112–143.

NGUYEN, M.Q., DELACHE, A., SIMOËNS, S., BOS, W.J.T. & EL HAJEM, M. 2016 Small scale dynamics of isotropic viscoelastic turbulence. *Phys. Rev. Fluids* **1** (8), 083301.

NI, R., OUELLETTE, N.T. & VOTH, G.A. 2014 Alignment of vorticity and rods with Lagrangian fluid stretching in turbulence. *J. Fluid Mech.* **743**, R3.

OLIVEIRA, P.J. 2024 A shear and elongational decomposition approach of the rate-of-deformation tensor for non-Newtonian flows with mixed kinematics. *J. Fluid Mech.* **1001**, A17.

OWOLABI, B.E., DENNIS, D.J.C. & POOLE, R.J. 2017 Turbulent drag reduction by polymer additives in parallel-shear flows. *J. Fluid Mech.* **827**, R4.

PASCHKEWITZ, J.S., DUBIEF, Y., DIMITROPOULOS, C.D., SHAQFEH, E.S.G. & MOIN, P. 2004 Numerical simulation of turbulent drag reduction using rigid fibres. *J. Fluid Mech.* **518**, 281–317.

POOLE, R.J. 2023 Inelastic and flow-type parameter models for non-Newtonian fluids. *J. Non-Newtonian Fluid Mech.* **320**, 105106.

POPE, S.B. 2000 *Turbulent Flows*. Cambridge University Press.

PROCACCIA, I., L'VOV, V.S. & BENZI, R. 2008 Colloquium: theory of drag reduction by polymers in wall-bounded turbulence. *Rev. Mod. Phys.* **80** (1), 225–247.

PTASINSKI, P.K., NIEUWSTADT, F.T.M., VAN DEN BRULE, B.H.A.A. & HULSEN, M.A. 2001 Experiments in turbulent pipe flow with polymer additives at maximum drag reduction. *Flow Turbul. Combust.* **66**, 159–182.

PUMIR, A. & WILKINSON, M. 2011 Orientation statistics of small particles in turbulence. *New J. Phys.* **13** (9), 093030.

UR REHMAN, S., LEE, J. & LEE, C. 2022 Effect of Weissenberg number on polymer-laden turbulence. *Phys. Rev. Fluids* **7** (6), 064303.

ROBERT, A., VAITHIANATHAN, T., COLLINS, L.R. & BRASSEUR, J.G. 2010 Polymer-laden homogeneous shear-driven turbulent flow: a model for polymer drag reduction. *J. Fluid Mech.* **657**, 189–226.

RYSKIN, G. 1987*a* Calculation of the effect of polymer additive in a converging flow. *J. Fluid Mech.* **178**, 423–440.

RYSKIN, G. 1987*b* Turbulent drag reduction by polymers: a quantitative theory. *Phys. Rev. Lett.* **59** (18), 2059.

SAMANTA, D., DUBIEF, Y., HOLZNER, M., SCHÄFER, C., MOROZOV, A.N., WAGNER, C. & HOF, B. 2013 Elasto-inertial turbulence. *Proc. Natl Acad. Sci. USA* **110** (26), 10557–10562.

SERAFINI, F., BATTISTA, F., GUALTIERI, P. & CASCIOLA, C.M. 2022 Drag reduction in turbulent wall-bounded flows of realistic polymer solutions. *Phys. Rev. Lett.* **129** (10), 104502.

SERAFINI, F., BATTISTA, F., GUALTIERI, P. & CASCIOLA, C.M. 2025 The role of polymer molecular weight distribution in drag-reducing turbulent flows. *J. Fluid Mech.* **1007**, A10.

SURESHKUMAR, R., BERIS, A.N. & HANDLER, R.A. 1997 Direct numerical simulation of the turbulent channel flow of a polymer solution. *Phys. Fluids* **9** (3), 743–755.

TABOR, M. & DE GENNES, P.G. 1986 A cascade theory of drag reduction. *Europhys. Lett.* **2** (7), 519.

TOMS, B.A. 1949 *Proceedings of the 1st International Congress On Rheology*, vol. II. Norm-Holland Publish Co.

TOMS, B.A. 1977 On the early experiments on drag reduction by polymers. *Phys. Fluids* **20** (10), S3–S5.

VALENTE, P.C., DA SILVA, C.B. & PINHO, F.T. 2014 The effect of viscoelasticity on the turbulent kinetic energy cascade. *J. Fluid Mech.* **760**, 39–62.

VALENTE, P.C., DA SILVA, C.B. & PINHO, F.T. 2016 Energy spectra in elasto-inertial turbulence. *Phys. Fluids* **28** (7), 075108.

VIRK, P.S., MICKLEY, H.S. & SMITH, K.A. 1970 The ultimate asymptote and mean flow structure in Toms' phenomenon. *J. Appl. Mech.* **37** (2), 488.

VIRK, P.S. 1975 Drag reduction fundamentals. *AIChE J.* **21** (4), 625–656.

WALEFFE, F. 1997 On a self-sustaining process in shear flows. *Phys. Fluids* **9** (4), 883–900.

WARHOLIC, M.D., MASSAH, H. & HANRATTY, T.J. 1999 Influence of drag-reducing polymers on turbulence: effects of Reynolds number, concentration and mixing. *Exp. Fluids* **27** (5), 461–472.

WARWARUK, L. & GHAEMI, S. 2024 Local flow topology of a polymer-laden turbulent boundary layer. *J. Fluid Mech.* **983**, A22.

WATANABE, T. & GOTOH, T. 2010 Coil-stretch transition in an ensemble of polymers in isotropic turbulence. *Phys. Rev. E—Stat. Nonlinear Soft Matter Phys.* **81** (6), 066301.

WATANABE, T. & GOTOH, T. 2013 Hybrid Eulerian–Lagrangian simulations for polymer–turbulence interactions. *J. Fluid Mech.* **717**, 535–575.

WHALLEY, R.D., PARK, J.S., KUSHWAHA, A., DENNIS, D.J.C., GRAHAM, M.D. & POOLE, R.J. 2017 Low-drag events in transitional wall-bounded turbulence. *Phys. Rev. Fluids* **2** (3), 034602.

WHITE, C.M., DUBIEF, Y. & KLEWICKI, J. 2012 Re-examining the logarithmic dependence of the mean velocity distribution in polymer drag reduced wall-bounded flow. *Phys. Fluids* **24** (2), 021701.

WHITE, C.M. & MUNGAL, M.G. 2008 Mechanics and prediction of turbulent drag reduction with polymer additives. *Annu. Rev. Fluid Mech.* **40** (1), 235–256.

WU, T. & BOS, W.J.T. 2022 Cascades of enstrophy and helicity in turbulence without vortex stretching. *Phys. Rev. Fluids* **7** (9), 094601.

WU, T. & BOS, W.J.T. 2021 Statistical mechanics of the Euler equations without vortex stretching. *J. Fluid Mech.* **929**, A11.

WU, T., DAVID, T. & BOS, W.J.T. 2023 Point-vortex statistical mechanics applied to turbulence without vortex stretching. *J. Stat. Mech.: Theory Exp.* **2023** (11), 113203.

XI, LI 2019 Turbulent drag reduction by polymer additives: fundamentals and recent advances. *Phys. Fluids* **31** (12), 121302.

XI, L. & GRAHAM, M.D. 2012 Dynamics on the laminar-turbulent boundary and the origin of the maximum drag reduction asymptote. *Phys. Rev. Lett.* **108** (2), 028301.

XU, C.X., ZHANG, Z.S. & NIEUWSTADT, F.T.M. 1996 Origin of high kurtosis in viscous sublayer. *Phys. Fluids* **8**, 1938–1942.

YARIN, A.L. 1997 On the mechanism of turbulent drag reduction in dilute polymer solutions: dynamics of vortex filaments. *J. Non-Newtonian Fluid Mech.* **69** (2–3), 137–153.